

Electrostatic Steering at Acetylcholine Binding Sites

Robert H. Meltzer,* Errol Thompson,* Kizhake V. Soman,* Xing-Zhi Song,* Jerry O. Ebalunode,[§] Theodore G. Wensel,[†] James M. Briggs,[§] and Steen E. Pedersen*

Departments of *Molecular Physiology and Biophysics and [†]Biochemistry and Molecular Biology, Baylor College of Medicine, Houston, Texas; and [§]Department of Biology and Biochemistry, University of Houston, Houston, Texas

ABSTRACT The electrostatic environments near the acetylcholine binding sites on the nicotinic acetylcholine receptor (nAChR) and acetylcholinesterase were measured by diffusion-enhanced fluorescence energy transfer (DEFET) to determine the influence of long-range electrostatic interactions on ligand binding kinetics and net binding energy. Changes in DEFET from variously charged Tb³⁺-chelates revealed net potentials of -20 mV at the nAChR agonist sites and -14 mV at the entrance to the AChE active site, in physiological ionic strength conditions. The potential at the $\alpha\delta$ -binding site of the nAChR was determined independently in the presence of *d*-tubocurarine to be -14 mV; the calculated potential at the $\alpha\gamma$ -site was approximately threefold stronger than at the $\alpha\delta$ -site. By determining the local potential in increasing ionic strength, Debye-Hückel theory predicted that the potentials near the nAChR agonist binding sites are constituted by one to three charges in close proximity to the binding site. Examination of the binding kinetics of the fluorescent acetylcholine analog dansyl-C6-choline at ionic strengths from 12.5 to 400 mM revealed a twofold decrease in association rate. Debye-Hückel analysis of the kinetics revealed a similar charge distribution as seen by changes in the potentials. To determine whether the experimentally determined potentials are reflected by continuum electrostatics calculations, solutions to the nonlinear Poisson-Boltzmann equation were used to compute the potentials expected from DEFET measurements from high-resolution models of the nAChR and AChE. These calculations are in good agreement with the DEFET measurements for AChE and for the $\alpha\gamma$ -site of the nAChR. We conclude that long-range electrostatic interactions contribute -0.3 and -1 kcal/mol to the binding energy at the nAChR $\alpha\delta$ - and $\alpha\gamma$ -sites due to an increase in association rates.

INTRODUCTION

Neuromuscular junction signal transduction involves the rapid binding of acetylcholine (ACh) to the nicotinic acetylcholine receptor (nAChR) followed by rapid clearance of ACh from the synapse by acetylcholinesterase (AChE) catalyzed hydrolysis. The ACh binding sites of both of these proteins are located within deep clefts, yet association with both proteins occurs at or near diffusion limited rates. One mechanism that may enhance the rate of cationic ligand binding to these proteins is long-range electrostatic attraction toward negatively charged surfaces near the ligand binding sites. Such electrostatic steering has been proposed as a mechanism for accelerating the rate of ligand association at the active site of AChE by concentrating the cationic ligands near the active gorge with an electronegative field (1,2). Early estimates using Brownian dynamics placed the magnitude of electrostatic steering as high as a 40-fold increase in

association rates (2). Subsequent computational refinements lowered this estimate to an increase of two- to sixfold (3), depending on ionic strength. These changes were consistent with the rates of binding of variously charged ligands upon successive mutagenesis of negatively charged surface residues on AChE (4).

The protein surfaces near the agonist binding sites of the nAChR have also been shown to be negatively charged: a local potential of -80 mV was measured in low ionic strength using the substituted cysteine accessibility method (5), and a potential of -15 mV was measured in physiological ionic strength using electron paramagnetic resonance (6). The binding affinity of the fluorescent agonist dansyl-C6-choline (DC6C) appears to be influenced by the electrostatic environment of the nAChR through two mechanisms. Direct electrostatic interactions that enhance binding of the ligand to the desensitized agonist site and indirect electrostatic interactions that affect the equilibrium between the resting and desensitized conformational states of the nAChR (7). The intrinsic decrease in desensitized-state affinity with increased ionic strength is about threefold (7). Raising ionic strength does not influence agonist dissociation kinetics at the $\alpha\delta$ -site, but decreases the dissociation rate by twofold at the $\alpha\gamma$ -site. The increased affinity and faster dissociation rate in low ionic strength at the $\alpha\gamma$ -site suggests that its association rate should be faster than the association rate for the $\alpha\delta$ -site; in physiological ionic strength, however, the association rates are indistinguishable between the two sites (8).

Submitted January 16, 2006, and accepted for publication May 17, 2006.

Address reprint requests to Steen E. Pedersen, Baylor College of Medicine, One Baylor Plaza, Houston, TX 77030. Tel.: 713-798-3888; E-mail pedersen@bcm.tmc.edu.

Robert H. Meltzer's present address is Dept. of Physiology & Biophysics, University of Alabama, Birmingham, AL.

Errol Thompson's present address is Dept. of Life Sciences, Winston-Salem State University, Winston-Salem, NC.

Kizhake V. Soman's present address is UTMB Bioinformatics Program and Dept. of Biochemistry & Molecular Biology, University of Texas Medical Branch, Galveston, TX.

© 2006 by the Biophysical Society

0006-3495/06/08/1302/13 \$2.00

doi: 10.1529/biophysj.106.081463

The quaternary ammonium common to nAChR agonists and to many antagonists is stabilized predominantly by interactions with aromatic π -electrons and not by direct charge neutralization or ion pair formation (9–11). However, the structure of the nAChR determined by electron-microscopic imaging of tubular crystalline arrays shows that anionic amino acids are concentrated near the agonist binding sites, with more negative charges present near the $\alpha\gamma$ -site than the $\alpha\delta$ -site (12). This suggests a role for the surrounding negative charges in accelerating the rate of agonist binding, particularly at the $\alpha\gamma$ -site at low ionic strength.

In the accompanying articles, the electrostatic environment within the ion-conductive pore of the nAChR was determined experimentally using diffusion-enhanced fluorescence energy transfer (DEFET) (13). We further took advantage of the well-developed theoretical basis of DEFET to compute expected changes in DEFET from the computed electrostatic potential (14–19). A direct comparison of experimentally determined potentials and the expected results from computed potentials revealed a consistent twofold or higher overestimate of computed potentials compared to the measured potentials. Although the exact basis of this discrepancy is unknown, it may reflect the limitations of continuum electrostatics computations in the constricted, concave environment of the nAChR channel where the charged residues are in close apposition to the fluorescence energy transfer acceptor (20). In contrast the ACh binding site entrances of AChE and the nAChR reside on a typically convex protein surface surrounded by negative surface charges.

In this article we apply the DEFET method to determine the contribution of the local potentials about the binding sites of the nAChR and AChE to agonist association rates and binding energies using fluorescent analogs as the DEFET acceptors. Experimental results were consistent with the potentials predicted by computational simulations. In addition, stopped-flow kinetic measurements of DC6C binding to the nAChR were used to determine the effect of electrostatic potentials on association rates. The data are consistent with a two- to threefold effect of long-range electrostatic attraction on association rates and binding constants.

MATERIALS AND METHODS

Materials

Dansyl-C6-Choline (DC6C) was synthesized as described previously (7,21). *N*-(7-nitro-2,1,3-benzoxadiazol-4-yl)-5-acylcholine (NBD-5-AC) was synthesized as described by Jurss et al. and Meyers et al. (22,23). Decidium, a bis-quaternary ethidium bromide analog with a 10-carbon methonium attachment (see Fig. 1) was synthesized as described by Berman et al. (24). *m*-Aminophenyl-trimethylammonium was synthesized according to Berman and Young (25). The luminescent terbium chelates, Tb^{3+} -EDTA ammonium (Tb^-), Tb^{3+} -*N*-(2-hydroxyethyl)ethylenediamine triacetate (Tb^0), and Tb^{3+} -*N,N'*-bis-(2-hydroxyethyl)ethylenediamine diacetate, bicarbonate (Tb^+) were prepared as described (13). All compounds synthesized within the lab had the expected properties as characterized by mass spectroscopy, absorbance

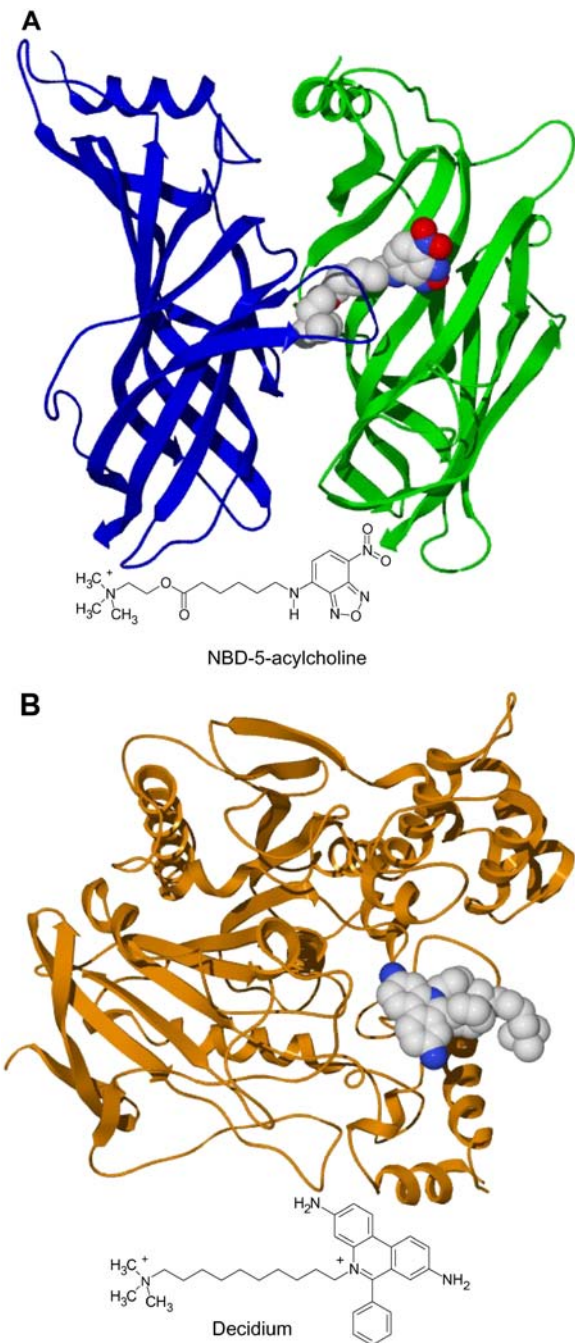


FIGURE 1 Fluorescent ligand structures. (A) NBD-5-AC is shown schematically and as a heavy-atom van der Waals structure as bound to the nAChR $\alpha\gamma$ -agonist binding site. The α -subunit is blue, the γ -subunit green; the other subunits were omitted for clarity. (B) Decidium is shown schematically and as bound to the *Torpedo californica* AChE catalytic site entrance. Structures and docking of ligands were determined as described in Materials and Methods.

spectra, fluorescence spectra, and, where appropriate, by binding to their targets.

nAChR and AChE were purified from *Torpedo californica* electric organ. nAChR enriched membranes were prepared as described (26,27). AChE was purified essentially as described by Taylor et al. (28); AChE was cleaved

with trypsin from crude *Torpedo* membranes, retained from the initial low-speed centrifugation step (26,27), and then purified by affinity chromatography using m-aminophenyl-trimethylammonium as the affinity ligand (25,28). Typical protein yield was 5–15 mg per preparation. AChE was pure as assessed by SDS-polyacrylamide gel electrophoresis (29) and by enzymatic activity measured using the Ellman assay (30).

Spectral and lifetime measurements

Tb³⁺-chelate spectra were measured as described previously (13). Absorbance spectra of 400 nM NBD-5-AC or decidium in the presence of 500 nM nAChR or AChE, respectively, were measured on a Cary 1/3 UV/VIS spectrophotometer (Varian, Sugarland, TX) in dual beam mode against reference samples without fluorophores. The R_0 values for energy transfer from Tb³⁺-chelates to NBD-5-AC and to decidium were determined as described for crystal violet in Meltzer et al. (13).

Lifetime determinations were carried out on a PhosphoCube lifetime instrument from HORIBA Jobin Yvon IBH or on an instrument using a mechanically chopped argon-ion laser as the excitation source, as described (13,31). Time-correlated photon counting of emitted light was collected through a 545-nm bandpass filter to monitor the peak Tb³⁺ emission. DEFET of Tb³⁺-chelates to NBD-5-AC was measured in 10 mM HEPES, pH 7.0, in HTPS (250 mM NaCl, 5 mM KCl, 3 mM CaCl₂, 2 mM MgCl₂, 20 mM HEPES, pH 7.0), or in 300 mM NaCl, 10 mM HEPES, pH 7.0. Some experiments were performed with buffers prepared in D₂O to increase the Tb³⁺-chelate lifetimes. NaCl titrations were performed in 25 × 5 × 5 mm stoppered glass cuvettes (Starna, Essex, England) by addition of 3 or 5 M NaCl in 10 mM HEPES, pH 7.0. All buffers were titrated to pH 7.0 immediately before the experiments and kept under argon to prevent exchange with atmospheric moisture.

DEFET measurements of electrostatic potential were performed by determining the second order rate constants of energy transfer, k_2^- , k_2^0 , and k_2^+ , from the changes in lifetimes of the variously charged Tb³⁺-chelates, Tb⁻, Tb⁰, and Tb⁺, with the addition of acceptor. k_2^x values, where x indicates the chelate charge, were calculated from either a single acceptor concentration or from the slope of a serial titration of NBD-5-AC into the nAChR as described previously (13): $k_2^x = (k_{\text{obs}} - k_0) / [\text{NBD} - 5 - \text{AC}]$ or $k_{\text{obs}} = k_2^x [\text{NBD} - 5 - \text{AC}] + k_0$ where $k_{\text{obs}} = 1/\tau_{\text{obs}}$. Samples often had a significant concentration of free, unbound NBD-5-AC that contributed to the DEFET signal. To correct the signal for unbound NBD-5-AC, its concentration was measured from the fluorescent intensity of samples and comparison to a standard curve, after clearing bound NBD-5-AC by centrifugation in a TOMY 150 MTX bench-top microcentrifuge. Energy transfer rates for bound NBD-5-AC were adjusted for the contribution of free NBD-5-AC as follows:

$$k_{2\text{adj}} = \frac{k_{2\text{obs}} - [\text{NBD}_{\text{free}}] / [\text{NBD}_{\text{total}}] * k_{\text{free}}}{1 - [\text{NBD}_{\text{free}}] / [\text{NBD}_{\text{total}}]} \quad (1)$$

The values for k_{free} were determined independently for each chelate. To distinguish the local potentials at the $\alpha\gamma$ - and $\alpha\delta$ -sites, 5 μM *d*-tubocurarine was added to specifically block the $\alpha\gamma$ -site. Lifetime measurements at the $\alpha\delta$ -site were then recorded in the presence or absence of 1 μM NBD-5-AC. The energy transfer rate k_2^x for each of the Tb³⁺-chelates was computed for the $\alpha\gamma$ -site ($k_{2\alpha\gamma}^x$) from the experimentally determined rates for the whole receptor ($k_{2\text{total}}^x$) and the $\alpha\delta$ -site ($k_{2\alpha\delta}^x$):

$$k_{2\alpha\gamma}^x = 2 * k_{2\text{total}}^x - k_{2\alpha\delta}^x \quad (2)$$

The electrostatic potential about the acceptor fluorophore was calculated from the energy transfer rates k_2^- , k_2^0 , and k_2^+ as described (13), using ratios ($\psi = k_{\text{B}}T \ln(k_2^+ / k_2^0) / e$) or the slope of $\ln(k_2^x)$ versus charge ($\psi = (k_{\text{B}}T / e) * (\text{slope of } \ln(k_2^x))$); the slope is determined by linear regression. Errors in k_2^x values were the mean \pm SE of several separate experiments; the error for the corresponding potential ψ (σ_ψ) was determined by propagation of errors (13). Charge number (z) and the mean distance of closest approach between charges and counterions (r) near the nAChR agonist binding site were

estimated by fitting changes in potential with ionic strength to the Debye-Hückel equation, Eq. 3.

$$\psi(I) = zq_e e^{-\kappa r} / 4\pi\epsilon\epsilon_0 r \frac{1}{\kappa} = \left(\frac{\epsilon\epsilon_0 RT}{2F^2} \right)^{0.5} I^{-0.5} \quad (3)$$

The potential at a given ionic strength $\psi(I)$ is a function of the elementary charge q_e , the polarizability of free space, ϵ_0 , the dielectric constant, ϵ , and the Debye length $1/\kappa$. The Debye length characterizes the screening effect of ionic strength on potential experienced about a point charge where R is the gas constant, F is Faraday's constant, and I is the ionic strength (for details also see Eq. 6 in Meltzer et al. (13)).

For experiments to determine the potential at the AChE active site, lifetime determinations were carried out in 1 mM Tris, pH 8.0, 10 mM Tris, pH 8.0, or in 40 mM MgCl₂, 100 mM NaCl, 10 mM Tris, pH 8.0. Tb³⁺-chelate concentrations were 4 or 8 mM; AChE concentrations were 10 or 20 μM ; decidium was titrated into samples in concentrations ranging from 0 to 10 μM . Luminescent decay rates (k_{obs}) were determined at each concentration and the rate constant for energy transfer, k_2^x , determined from the slope of k_{obs} versus decidium concentration as described above; only data up to 4.5 μM decidium was included because higher concentrations displayed deviations consistent with the presence of free decidium. Potentials were computed from matched titrations of the three chelates using the slope of $\ln(k_2^x)$ versus charge (13). The errors of the k_2^x and the electrostatic potentials are the averages and ranges of several individual experiments.

Computational modeling

The atomic-resolution homology structure of the nAChR described in the accompanying article (14) was used to model the binding of NBD-5-AC. The quaternary ammonium of NBD-5-AC was positioned in the nAChR $\alpha\gamma$ - and $\alpha\delta$ -binding sites according to the position of the carbamylcholine ammonium in the structure of AChBP and then energy minimized using the MM+ parameter set implemented in Hyperchem (vs. 5.1, Hypercube, Gainesville, FL). The crystallographic coordinates of decidium bound to the mouse AChE (accession No. 1J07) (32) were transferred into the structure of *Torpedo* AChE. (NCBI accession No. 1EA5 (33)). As the residues in the vicinity of decidium are identical in mouse and *Torpedo* AChE, the resulting decidium-bound structure was used without further refinement.

Computational methods for assigning partial charges, determining electrostatic potentials, and computing DEFET rates were applied essentially as described (14). The charge distribution of decidium and NBD-5-AC were determined by semiempirical quantum mechanics in Hyperchem using the AM1 Hamiltonian. Protein partial charges were assigned using the University of Houston Brownian dynamics program (UHBD) implementation of the Bashford and Karplus method (34). The electrostatic potentials were computed with UHBD at 20 mM or 300 mM ionic strength using the nonlinear Poisson-Boltzmann equation (35). Several iterations were carried out using decreasing grid sizes with the boundary conditions defined from the previous iterations. This produces a grid in the vicinity of the binding site with sufficient resolution for computation of k_2^x values without loss of long-range electrostatic information.

The bimolecular rate constants (k_2^x) for DEFET from charged Tb³⁺-chelates were computed by numerical integration (15) over a 65 × 65 × 65 point grid that was spaced at 0.75 Å and centered on the acceptor chromophore. The chelate radius was assumed to be 5 Å. The distance to the acceptor fluorophore was measured from the chelate center to the nearest atom in the chromophore of either NBD-5-AC or decidium. The integration included the electrostatic effects of the Poisson-Boltzmann calculation on the local chelate concentration (see Eq. 7 in Meltzer et al. (14)) for each chelate. These k_2^x values, in turn, can be used to compute a potential in the same manner as for experimental k_2^x values, and provides a point of direct comparison between experimentally determined and computed potentials. Directly comparing the k_2^x values is impractical because the numerical integration is highly sensitive to assumptions of chelate radius and other

factors. These factors tend to cancel upon calculating a potential from the ratio of k_2^x values. The potential is, therefore, a more robust point of comparison (14). Direct comparison of the Poisson-Boltzmann calculation with the potentials from experimental k_2^x measurements may be misleading because the k_2^x values reflect an integrated effect of the potential over the volume where energy transfer can occur and, thus, does not correspond directly to any single potential value.

nAChR binding assays

NBD-5-AC binding to nAChR membranes was measured by inhibition of the initial rate of ^{125}I - α -Bungarotoxin binding, essentially as described (36). nAChR was first treated with diisopropyl fluorophosphonate (Aldrich Chemical, Milwaukee, WI) to inactivate AChE. Binding was for 45 min in 1 nM ^{125}I - α -Bungarotoxin in HTPS buffer and with varying concentrations of NBD-5-acylcholine. The reactions were quenched by the addition of 300 nM α -bungarotoxin, filtered, and counted. IC50s were determined by fitting to a single site inhibition curve (37).

DC6C association kinetics were determined by fluorescence enhancement upon binding, using energy transfer from nAChR tryptophan residues, after rapid mixing on a model SF-2001 stopped-flow instrument from Kintek (Austin, TX) (8). Kinetics were determined in 20 mM HEPES at pH 7.0 with varying NaCl concentrations, in the presence or absence of 10 μM proadifen. Fluorescence was excited at 290 nm with a 4-nm slit width using a 75W xenon lamp; emission was measured through a 495-nm cut-on filter (Oriol 59492). Kinetic traces were fitted to a three exponential equation:

$$F = A_1 e^{k_1 t} + A_2 e^{k_2 t} + A_3 e^{k_3 t} + C, \quad (4)$$

where F is the observed fluorescence intensity, k_1 , k_2 , and k_3 are the rate constants of the fast, intermediate, and slow association components, and A_1 , A_2 , and A_3 are their respective amplitudes. C represents the background fluorescence. The ionic strength dependence of the fast association rate was analyzed using an equation derived from Debye-Hückel theory, Eq. 5, (7,38) to estimate the number (z_R) and mean distance of closest approach of charges (r) near the ACh binding sites.

$$\log k = \log k_0 - (2A z_R z_L I^{0.5}) / (1 + r B I^{0.5}). \quad (5)$$

RESULTS

Electrostatic steering is a mechanism for enhancing the binding rate and affinity of ionic ligands by a distribution of counter charges that evoke an attractive potential field. One of the best characterized examples of electrostatic steering is the binding of ACh to AChE, and this mechanism may also serve to enhance ACh-binding to the nAChR. To determine the contribution of electrostatic potentials to nAChR-binding energy and kinetics, we first determined the electrostatic potentials at the sites by diffusion-enhanced fluorescence energy transfer (DEFET). We also determined the potential at the AChE active-site entrance by DEFET measurements to correlate experimental potentials with the extensive extant enzymatic and computational work on AChE.

Applying the DEFET approach required energy transfer acceptors located at these sites. NBD-5-AC is a high-affinity nAChR agonist that has spectral overlap with Tb^{3+} -emission (22,23). We modeled the binding of this ligand to the *Torpedo* AChR on the basis of the crystal structure of carbamylcholine bound to AChBP as described in Materials

and Methods (Fig. 1 A). The NBD fluorophore was localized to solvent-exposed regions at the ACh-binding site entrances. The high-affinity, bis-quaternary, AChE inhibitor decidium binds near the entrance to the mouse AChE active site (32). A model for decidium bound to *Torpedo* AChE (Fig. 1 B) was constructed by combining the crystal structures of *Torpedo* AChE and of decidium bound to the mouse AChE. After synthesizing NBD-5-AC and decidium, their energy transfer parameters as acceptors of Tb^{3+} -chelate luminescence were characterized.

Energy transfer efficiency of donor-acceptor pairs

The efficiency of energy transfer between two fluorophores is characterized by the Förster distance (R_0), the distance at which energy transfer is 50% efficient. R_0 was computed from the optical properties of Tb^+ , Tb^0 , and Tb^- as the energy transfer donors and NBD-5-AC and decidium as acceptors (Table 1). The spectral overlap integral J represents the overlap of donor luminescence emission spectrum with the acceptor absorbance spectrum and is required to determine R_0 ; these spectra are shown in Fig. 2. Notably, the spectrum for decidium bound to AChE is shifted 20 nm to the red compared with free decidium (not shown). The R_0 values for the donor-acceptor pairs are $\sim 33 \text{ \AA}$ for energy transfer to NBD-5-AC and $\sim 31 \text{ \AA}$ for Tb^{3+} -chelate energy transfer to bound decidium. The R_0 values for free decidium are near 28 \AA (data not shown). The uncertainties listed in Table 1 are due to the possible variation in the dipole orientation factor κ^2 . The R_0 values were utilized primarily for numerical integration of the DEFET rates, k_2^x ; κ^2 values were computed explicitly at each grid point in the computation, thereby eliminating the effect of the uncertainty in R_0 on the integrated result.

Local electronegative potentials at the nAChR agonist sites

We first determined the binding affinity of NBD-5-AC for the nAChR so that we could design the experimental

TABLE 1 Fluorescence energy transfer parameters

	Tb^+	Tb^0	Tb^-
η		1.33	
κ^2		1/3–4/3	
Q_0	0.182	0.187	0.224
	NBD-5-AC		
$J \text{ (M}^{-1}\text{cm}^3\text{)}^*$	3.80×10^{-14}	3.75×10^{-14}	3.83×10^{-14}
$R_0^\dagger \text{ (\AA)}$	33.2 ± 5.4	33.2 ± 5.4	34.9 ± 5.7
	Decidium		
$J \text{ (M}^{-1}\text{cm}^3\text{)}^*$	2.36×10^{-14}	2.34×10^{-14}	2.29×10^{-14}
$R_0^\dagger \text{ (\AA)}$	$30.6 \pm 5.$	$30.7 \pm 5.$	$32. \pm 5.$

*The values J , Q_0 , η , and κ^2 were determined as described in Materials and Methods; values for J were computed from the spectra of the bound ligand determined in water.

$^\dagger R_0$ was computed for the minimum and maximum values of κ^2 ; the average and range are presented.

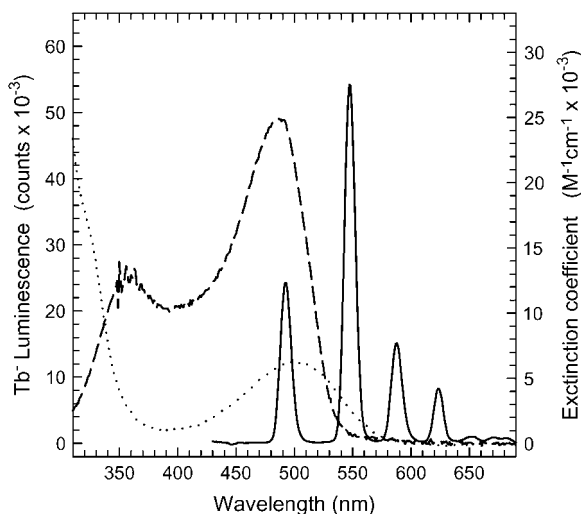


FIGURE 2 Spectral overlap of Tb^{3+} emission with decidium and NBD-5-AC absorbance. The emission spectrum of 1 mM Tb^{3+} (solid line) was measured with excitation at $\lambda_{\text{ex}} = 370$ nm. Absorbance spectra were measured for 400 nM NBD-5-AC bound to nAChR (500 nM, dashed line) and for 2.1 μM decidium bound to 5 μM AChE (dotted line) as described in Methods and Materials; extinction coefficients were calculated from the measured absorbance and the fluorophore concentration.

conditions to minimize the free ligand concentration and the energy transfer to unbound NBD-5-AC. A K_D of 33 ± 3 nM was determined by inhibition of the initial rate ^{125}I -Bungarotoxin binding to the nAChR in HTPS; in the presence of 25 μM tetracaine, the K_D was 47 ± 4 nM; in the presence of the desensitizing noncompetitive antagonist proadifen, the K_D was 15.4 ± 2.7 nM.

The electrostatic potentials at the agonist binding sites of the *Torpedo californica* nAChR were determined from the changes in DEFET rates, k_2^+ , k_2^0 , and k_2^- , to bound NBD-5-AC with the change in charge of the three corresponding Tb^{3+} chelates, Tb^+ , Tb^0 , and Tb^- . The observed DEFET rate is measured from the changes in luminescent decay rate in the absence and presence of acceptor, as shown in Fig. 3 A. The change in decay rate is proportional to the acceptor concentration and higher concentrations yield more robust changes. Reliable determinations of DEFET rates required μM concentrations of free NBD-5-AC; therefore, DEFET measurements to bound NBD-5AC required similar or higher nAChR concentrations. To improve sensitivity and to minimize artifacts from the strongly scattering membrane suspension, we carried out experiments in D_2O , rather than H_2O (39). This is shown in Fig. 3 A where decays in the presence and absence of 3 μM NBD-5-AC are compared for H_2O and D_2O . Experiments in D_2O had lifetimes about three times longer than in H_2O and had greater changes in decay rate at the same NBD-5-AC concentration. DEFET rates (k_2^x) are independent of chelate lifetime and we could, therefore, combine k_2^x data from experiments carried out in either H_2O or in D_2O .

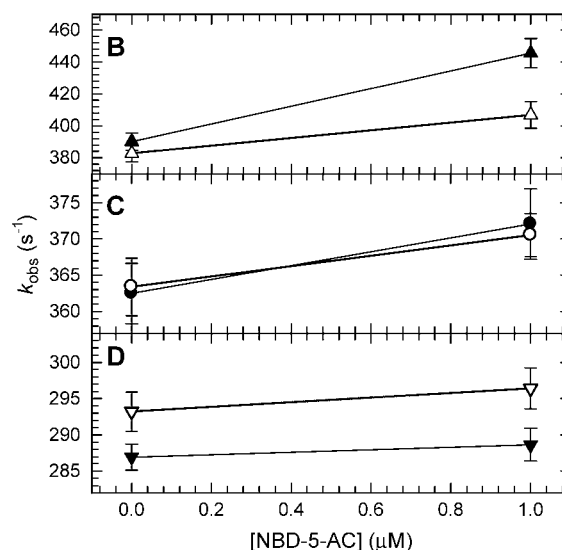
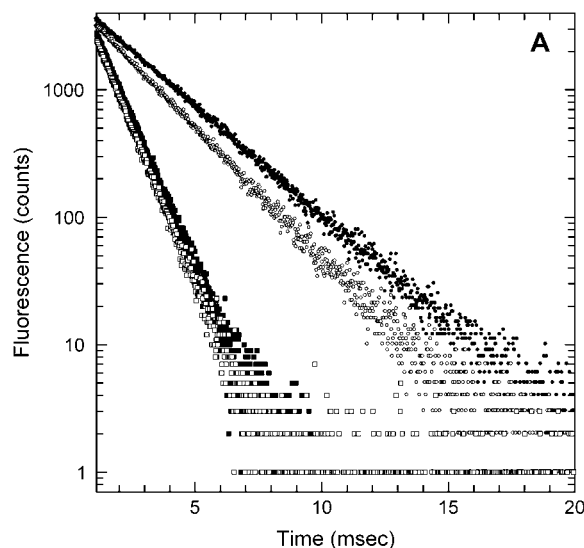


FIGURE 3 D_2O enhances Tb^{3+} -chelate lifetimes. (A) Luminescence decays of 1 mM Tb^{3+} were measured as described in Materials and Methods in the absence (\bullet , \blacksquare) or presence (\circ , \square) of 3 μM NBD-5-AC in 10 mM HEPES prepared in D_2O (\circ , \bullet) or H_2O (\square , \blacksquare). (B, C, D) Energy transfer from Tb^{3+} -chelates to NBD-5-AC bound to nAChR. The luminescence decays (k_{obs}) of (B) Tb^+ (\blacktriangle , \triangle), (C) Tb^0 (\bullet , \circ), and (D) Tb^- (\blacktriangledown , \triangledown) were measured in 10 mM HEPES (\blacktriangle , \bullet , \blacktriangledown) or in 10 mM HEPES, 300 mM NaCl (\triangle , \circ , \triangledown) prepared in D_2O . Measurements were made in the presence of 2 μM nAChR agonist binding sites with or without 1 μM NBD-5-AC, in paired samples. Note the changes in scale among B, C, and D. Errors bars are the mean \pm SE of $n = 3$ samples.

The electrostatic potential for free NBD-5-AC as calculated from DEFET rates k_2^+ , k_2^0 , and k_2^- , indicated a local potential of 5.1 mV in low ionic strength solution (Table 2). This value is smaller than that observed for free crystal violet (13), for ethidium (17), or for decidium (see below), but can be explained by the distance between the fluorophore and the cationic center in NBD-5-AC (see Fig. 1 A), unlike the other acceptors where the cation is integral to the fluorophore. The potential at the nAChR agonist sites was determined from the

TABLE 2 Energy transfer and local potential determined near NBD-5-AC and the nAChR agonist binding sites

	<i>I</i> (mM)	Experimental k_2^x ($\mu\text{M}^{-1} \text{s}^{-1}$)*			ψ (mV) [†]
		k_2^+	k_2^0	k_2^-	
NBD-5-AC	6	25.3 ± 1.1 (3)	29.8 ± 1.0 (3)	37.8 ± 1.2 (3)	5.1 ± 0.9
nAChR	6	57.0 ± 2.9 (7)	11.7 ± 0.5 (8)	2.9 ± 0.4 (8)	−37.9 ± 2.1
$\alpha\delta$ -site [‡]	6	38.8 ± 1.1 (5)	14.9 ± 0.6 (5)	5.1 ± 1.0 (5)	−25.7 ± 2.5
$\alpha\gamma$ -site (calculated)	6	75.2 ± 1.4	8.4 ± 0.8	0.6 ± 0.4	−60.4 ± 8.8
nAChR	300	35.5 ± 1.1 (6)	13.5 ± 0.6 (6)	6.1 ± 0.4 (6)	−22.4 ± 1.2
$\alpha\delta$ -site [‡]	300	33.2 ± 2.2 (4)	14.3 ± 0.7 (4)	10.9 ± 0.9 (4)	−14.2 ± 1.6
$\alpha\gamma$ -site (calculated)	300	37.7 ± 2.4	12.7 ± 0.9	1.3 ± 1.0	−42.7 ± 10.0
		Computed k_2^x ($\mu\text{M}^{-1} \text{s}^{-1}$) [§]			
	<i>I</i> (mM)	k_2^+	k_2^0	k_2^-	ψ (mV) [†]
NBD-5-AC	20	13	15.6	19.8	5.3
nAChR	20	24.5	3.6	1.4	−36.3
$\alpha\delta$ -site	20	8.6	4.3	2.5	−15.7
$\alpha\gamma$ -site	20	40.3	2.9	0.3	−62.2
nAChR	300	6.6	3.6	2.6	−12.1
$\alpha\delta$ -site	300	5.2	4.3	3.9	−3.7
$\alpha\gamma$ -site	300	8	2.9	1.2	−24.5

* k_2^x values were determined from Tb³⁺-chelate lifetime determinations in 3 μM nAChR suspensions, before and after addition of 1 μM NBD-5-AC, as described in Materials and Methods; the values were corrected for free NBD-5-AC.

[†]Local potentials were computed from experimental or computed k_2^x values and the corresponding errors determined by propagation of errors.

[‡] k_2^x values for the $\alpha\delta$ -site were determined from samples including 5 μM *d*-tubocurarine to block the $\alpha\gamma$ -site.

[§]Computed k_2^x values were determined from the structure of NBD-5-AC alone or bound to either the $\alpha\gamma$ -site or $\alpha\delta$ -site. The nAChR k_2^x values were computed from the average of both k_2^x values.

k_2^+ , k_2^0 , and k_2^- values calculated from decay rates taken in the absence or presence of 1 μM NBD-5-AC as shown in Fig. 3B. These values were further corrected for energy transfer to residual free NBD-5-AC using Eq. 1. The free NBD-5-AC concentration was determined from fluorescence of the sample after clearing bound NBD-5-AC by centrifugation and was routinely <10%. The corrected values for k_2^+ , k_2^0 , and k_2^- are summarized in Table 2. The binding sites have a net potential of −38 mV in low ionic strength that is decreased to −22 mV in physiological ionic strength buffer. The change in k_2^0 values from free to bound NBD-5-AC indicates the relative accessibility of the fluorophore upon binding; this was only a 50% decrease, indicating that the bound NBD fluorescent group remains largely solvent accessible, an observation that is consistent with the structural model in Fig. 1A.

Agonists bind cooperatively to the nAChR, and therefore, we would expect the $\alpha\gamma$ - and $\alpha\delta$ -sites to be equally occupied by NBD-5-AC during the DEFET experiments described above (8). Thus, the measured potential should reflect contributions from both sites. To determine whether the electrostatic potential differed significantly between the two sites, we determined the DEFET rates at the $\alpha\delta$ -site by selectively blocking the $\alpha\gamma$ -binding site with *d*-tubocurarine (40,41). From the DEFET measurements taken at the $\alpha\delta$ -site and at both sites, the energy transfer rates and local potentials at the $\alpha\gamma$ -binding site were calculated as described in Materials and Methods (Eq. 2). The data in Table 2 show a substantially smaller potential at the $\alpha\delta$ -site in both high and

low ionic strength buffers. The calculated k_2^x values and voltage at the $\alpha\gamma$ -site are concomitantly larger in magnitude. These data suggest that most of the observed net potential was derived from the $\alpha\gamma$ -site, −60 mV in low ionic strength and −43 mV in physiological ionic strength.

Computational simulation of agonist site electrostatic potentials

To determine whether these measured potentials were consistent with computed potentials, we computed Poisson-Boltzmann electrostatic surface potentials from the structural models of NBD-5-AC bound to the nAChR $\alpha\gamma$ - and $\alpha\delta$ -agonist binding sites and of free NBD-5-AC using the UHBD program. The computed potentials were then used to calculate the expected DEFET rates for each ACh binding site by numerical integration of the DEFET equation as described in Materials and Methods and in Meltzer et al. ((14); Eq. 7). This approach directly compared computed and experimental DEFET rates and potentials. As observed previously (14), the computed DEFET rates were sensitive to the values assumed for several parameters, such as chelate size. Nonetheless, the voltages calculated from the rates were relatively robust because these parameters affected all three chelates in a systematically similar way and the effects cancel when computing the potential (42). Here, we assumed a chelate radius of 5 Å, which is close to the value obtained from molecular modeling of the chelates.

The computed DEFET rates and the corresponding voltages as calculated from the ratios of the DEFET rates are given in Table 2. The computed k_2^0 value for free NBD-5-AC was twofold lower than the experimental k_2^0 , indicating that the integration yielded a reasonable approximation for the simplest case of free acceptor, without charge effects, and in the absence of protein. The corresponding voltage of 5.3 mV agrees closely with the experimental value, 5.1 mV, further substantiating the validity of the integration. For nAChR-bound NBD-5-AC, computed k_2^0 values were up to fourfold lower than the corresponding experimental values. Comparing k_2^0 values for free NBD-5-AC to bound NBD-5-AC ($k_{2\text{free}}^0 : k_{2\text{bound}}^0$) indicates the extent of shielding of the fluorophore from solvent. Comparison of the experimental k_2^0 values shows this ratio to be ~ 2.5 ; the computed values yield a ratio of ~ 4.3 , indicating that the structural binding model somewhat overestimates the extent of shielding of the chromophore.

The potentials calculated from the computed k_2^- , k_2^0 , and k_2^+ values for low ionic strength show good agreement with the experimental values for the $\alpha\gamma$ -site and for the net potential, whereas the $\alpha\delta$ -site potential is underestimated by 40%. For high ionic strength, the discrepancies are larger; the computed values underestimated experimental potentials twofold or more. Comparison of the computed potentials at low and high ionic strength show stronger screening by ionic strength than occurs experimentally. At physiological ionic strength, the computational and experimental determinations of k_2^x values suggest that the protein surface charge distribution contributes a two- to fivefold increase in the local cation concentration at the $\alpha\gamma$ -site and very little increase at the $\alpha\delta$ -site.

Charge number and distribution from ionic strength perturbation

An alternative approach to analyzing the electrostatic environment of the agonist binding sites is to determine the variation of the potential with ionic strength. DEFET rates were measured during titration of increasing NaCl concentrations for NBD-5-AC in the presence or absence of excess nAChR for each of the three Tb^{3+} -chelates (Fig. 4). The energy transfer rates k_2^+ , k_2^0 , and k_2^- are shown for NBD-5-AC free in solution (Fig. 4 A) and bound to the nAChR (Fig. 4 B). The influence of the negative potentials near the agonist sites is apparent from the larger difference between k_2^+ and k_2^- for bound NBD-5-AC as compared with free NBD-5-AC. The local potentials at each ionic strength condition were computed from ratios of the rates and plotted versus ionic strength in Fig. 4 C. Fits of the Debye-Hückel equation (Eq. 3) to the potential estimates the number and distribution of charged amino acids near the site of NBD-5-AC binding. Best fits of Eq. 3 to free NBD-5-AC-potentials gave $z = 0.13 \pm 0.03$ and $r = 4.4 \pm 0.7 \text{ \AA}$. For bound NBD-5-AC, $z = -0.74 \pm 0.2$ and $r = 3.1 \pm 0.7 \text{ \AA}$ (see Table 4).

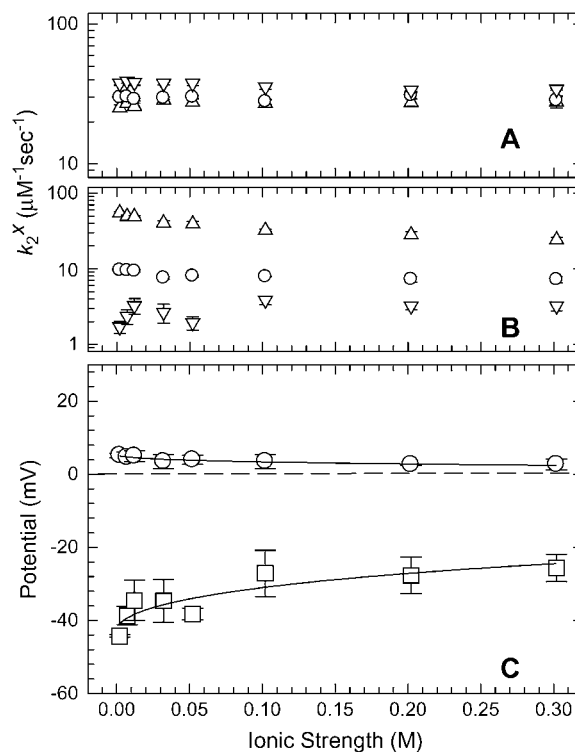


FIGURE 4 NaCl screens the electrostatic potential at nAChR agonist sites. Energy transfer rates (k_2^x) were calculated from luminescent decay rates for Tb^{3+} (Δ), Tb^0 (\circ), and Tb^- (∇) determined in the absence or presence of 1 μM NBD-5-AC. Measurements were made for NBD-5-AC either (A) free or (B) bound to 2 μM nAChR agonist sites. Ionic strength was varied by titration of NaCl into 10 mM Hepes, D_2O as described in Materials and Methods. Error bars represent mean \pm SE ($n = 3$). (C) The electrostatic potential at each ionic strength was calculated as described in Materials and Methods for free NBD-5-AC (\circ) and for bound NBD-5-AC (\square). Errors were calculated by propagation of error from mean \pm SE of the energy transfer rates. The change in potential with respect to ionic strength was fitted to Eq. 3 (lines).

The influence of the charge distribution on agonist binding kinetics

To evaluate the effect of long-range electrostatic attraction on the kinetics of binding, we determined the association rates for the fluorescent agonist DC6C in varying ionic strengths. When the nAChR is rapidly mixed with DC6C in the stopped-flow, binding kinetics in high ionic strength are dominated by slow conformational changes that can be fitted to three exponentials (see Fig. 5 A, right trace). The fastest exponential component corresponds to direct binding to preexisting desensitized receptors; it reflects the intrinsic association rate and is the rate of interest. At the highest ionic strength, this component is a small fraction (5–20%) of the total fluorescence change; however, as the ionic strength decreases, more receptors preexist in a desensitized state and the amplitude of this fast component is increased and the association trace appears shifted to the left (Fig. 5 A). Binding kinetics were also measured in the presence of 10 μM

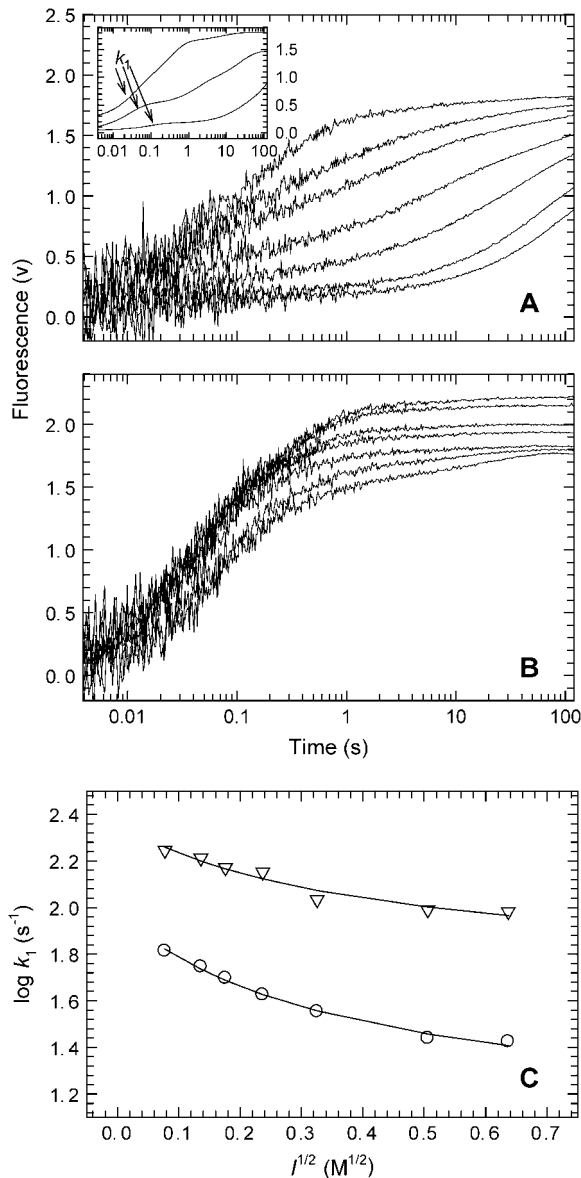


FIGURE 5 Association kinetics of DC6C binding to the nAChR. DC6C binding was measured by rapidly mixing 400 nM DC6C with an equal volume of 40 nM nAChR binding sites as described in Materials and Methods in the absence (A) or presence (B) of 10 μ M proadifen. NaCl concentrations were 1, 12.5, 25, 50, 100, 250, and 400 mM. Higher NaCl concentrations shift the association curves downward and to the right in both experiments. Each kinetic trace was fitted to the three-exponential equation (Eq. 4); the inset shows fits for 1, 50, and 400 mM NaCl from panel A. The initial rates of association, k_1 , in the presence of proadifen (○, from panel B), or the absence of proadifen (▽, from separate data collected using 200 nM nAChR and 2 μ M DC6C) were plotted versus ionic strength (C) and fitted to the Debye-Hückel equation (Eq. 5).

proadifen (Fig. 5 B), which stabilizes the desensitized state and shows a higher amplitude for the fast component at all ionic strengths.

The first rate terms of three-exponential fits (Eq. 4), k_1 (see inset in Fig. 5 A), are plotted versus ionic strength in Fig. 5 C for the data in the presence of proadifen (Fig. 5 B) and for

data in the absence of proadifen collected at higher DC6C concentrations; the rates change 1.5- to 2-fold from low to physiological ionic strength. Fits to the Debye-Hückel equation (Eq. 5; see also Eq. 6 in the accompanying paper, Meltzer et al. (13)) were used to extract the effective charge number (z) and mean distance of closest approach (r). Agonist association to the nAChR in the absence of proadifen was characterized by a charge distribution of $z = -1.6$ and $r = 7.6$ Å; in the presence of proadifen, $z = -2.4$ and $r = 8.1$ Å. The effective electrostatic potential that influences agonist association represents ~ 2 acidic residues in proximity to the agonist binding sites. This result differs from the Debye-Hückel analysis of potentials derived from DEFET measurements that indicate only -0.7 charges over a smaller distribution.

Electrostatic potential at the AChE active site cleft

The local potential near the cleft to the AChE active site was measured experimentally by determining the influence of the local potential on the distribution of the Tb³⁺-chelates near the fluorescent AChE inhibitor decidium. Because AChE is soluble and scatters less light than the AChR-rich vesicles, we could carry out experiments by titration of the ligand into high, 10–20 μ M AChE concentrations, as illustrated in Fig. 6. Tb³⁺ decay rates, k_{obs} , from titrations of free decidium into low ionic strength buffer are plotted in Fig. 6 A and the DEFET rates, k_2^+ , k_2^0 , and k_2^- , determined from the slopes. The slopes were steepest for Tb⁻ and shallowest for Tb⁺, consistent with the presence of a positive potential at the bis-cationic decidium. The DEFET rates, k_2^x , and corresponding potentials for free decidium are given in Table 3; increasing the ionic strength to physiological levels decreases the potential from +14 to +6 mV.

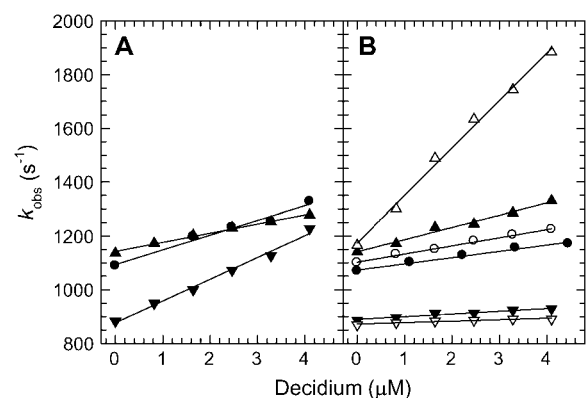


FIGURE 6 Energy transfer from Tb³⁺-chelates to decidium and to the decidium-AChE complex. (A) Decidium was titrated into 8 mM Tb³⁺ (▲), Tb⁰ (●), or Tb⁻ (▼) in 10 mM Tris buffer and the luminescent decay rate, k_{obs} , determined at each concentration. (B) Decidium was titrated into solutions of 20 μ M AChE with 4 mM Tb³⁺-chelate in either 10 mM Tris buffer (Δ, ○, ▽) or in 40 mM MgCl₂, 100 mM NaCl, 10 mM Tris (▲, ●, ▼). The decay rates are plotted for titrations into Tb⁺ (Δ, ▲), Tb⁰ (○, ●), and Tb⁻ (▽, ▼). The solid lines show the best linear fits; the slopes equal k_2^x .

Energy transfer measurements were performed similarly to AChE-bound decidium (Fig. 6 B, Table 3). The steepest slopes, and largest k_2 values, are for the positive chelate, Tb^+ , indicative of a negative potential. This pattern of slopes is similar in high and low ionic strength, but the changes in slope were smaller in higher ionic strength, which reflects a smaller negative potential. The energy transfer from Tb^0 , k_2^0 , decreases by 50% from free decidium to AChE-bound decidium. This change reflects the relative steric accessibility of decidium upon binding and shows that the acceptor fluorophore remains largely solvent exposed, consistent with the bound structure (Fig. 1 B). In low ionic strength conditions, the data indicate in a local potential of -33 mV that decreases to -14 mV in high ionic strength conditions.

To determine whether the electrostatic field computed by Poisson Boltzmann continuum electrostatics agreed with these measurements, we used the computed potential to determine the expected k_2^x values by numerical integration, using the methods presented in the accompanying article (14), and further used the ratio of those values to calculate a local potential. This value could then be compared directly to the voltages determined from the ratio of measured values. Although the integrated k_2^x values differ from the measured values by up to fourfold (see Table 3), the resultant potentials agree with the measured potentials within 30%. In addition, the change in computed k_2^0 from free to bound decidium is 50%, which agrees with the measured change in k_2^0 .

DISCUSSION

Protein-cation interactions are stabilized through electrostatic interactions, often by formally neutral groups such as backbone carbonyls in the selectivity filters of voltage-gated potassium channels (43) or aromatic ring π -electrons in the binding pocket of the nAChR (10). In addition, surface charge distributions may stabilize cationic ligand binding by enhancing association kinetics. We utilized DEFET mea-

surements to determine whether long-range electrostatic interactions influence the binding affinity and association kinetics of ACh to the nAChR. We found that ACh binding to the $\alpha\gamma$ - and $\alpha\delta$ -sites of the nAChR are stabilized by -1 and -0.3 kcal/mol, respectively, in physiological ionic strength (see calculation below). Electrostatic attraction increases the association rate to a corresponding extent with no change in the dissociation rates (8). Ionic strength screens the influence of the charge density in the vicinity of the binding sites. The experimental results were largely consistent with the predictions based on the Poisson-Boltzmann continuum electrostatic calculations. Thus, long-range electrostatic attraction constitutes a small but measurable component of ACh binding.

Electrostatics of nAChR agonist binding sites

We utilized the DEFET technique to measure surface electrostatic potentials because this method provides a direct comparison of three chelates that vary in charge but are nearly isosteric and have nearly identical optical properties. As DEFET donors, they can be compared directly with each other without concern for differences in solubility, protein interaction, reactivity, or chemical composition. The change in DEFET rates with charge directly reflects the change in local concentration due to long-range electrostatic interactions rather than short-range interactions such as van der Waals interactions, ion-pair formation, or dehydration. A second, distinct advantage of the DEFET approach is that the second order rate constants, k_2^x , can be computed by integration of the accessible volume surrounding the acceptor and include the influence of electrostatic interactions (15). Thereby, DEFET data can be compared directly with the results from standard computations, such as continuum Poisson-Boltzmann electrostatics, to provide a cross-check between electrostatic computation and experiment.

TABLE 3 Energy transfer and potential determined near decidium and AChE

	<i>I</i>		Experimental k_2 ($\mu\text{M}^{-1} \text{s}^{-1}$)*			ψ mV [†]
	mM	k_2^+	k_2^0	k_2^-		
Free decidium	4, 13 [‡]	30 ± 2 (2)	52.8 ± 0.1 (2)	89 ± 5 (2)	13.9 ± 1.4	
Free decidium	230	38 ± 1 (2)	49 ± 4 (2)	63 ± 2.7 (2)	6.3 ± 0.9	
AChE + decidium	9, 13 [‡]	122 ± 55 (2)	28 ± 3 (2)	8.2 ± 2.7 (2)	-33 ± 10	
AChE + decidium	230	43 ± 2 (2)	23.4 ± 0.3 (2)	13.6 ± 3.5 (3)	-14 ± 5	
		Computed k_2 ($\mu\text{M}^{-1} \text{s}^{-1}$) [§]				
		k_2^+	k_2^0	k_2^-		
Free decidium	20	8	14.9	18.4	16	
AChE + decidium	20	46	7.3	1.7	-42	
AChE + decidium	300	12	7.3	4.9	-11	

*Experimental k_2^x values were determined from (*n*) serial decidium titrations, carried out essentially as shown in Fig. 6, at the indicated ionic strengths. Titrations in the presence of 10 or 20 μM AChE spanned 0–4 μM decidium; in the absence of AChE, titrations were to 10 μM decidium.

[†]Local potentials were calculated from experimental or computed k_2^x as described in Materials and Methods.

[‡]Data were combined from two experiments at different ionic strengths.

[§]Computed k_2^x values were determined from the structure of decidium itself or as bound to AChE as described in Materials and Methods.

The data show the presence of small negative potentials of -14 and -42 mV for the two agonist sites, at physiological ionic strength. These values are not strikingly different from the data of Addona et al. (6) who determined a -15 mV potential using EPR after reacting a spin label at the agonist sites. In contrast, Stauffer and Karlin (5) determined a potential of -80 mV from the reactivity of variously charged methanethiosulfonate compounds with the reduced disulfide of the agonist site. However, their value is for zero ionic strength and, therefore, not inconsistent with the low ionic strength value -60 mV determined here for the $\alpha\gamma$ -site. In addition, the reduced cysteines may themselves have contributed to the measured potentials

The negative potentials contribute to larger binding energies for the $\alpha\gamma$ - and $\alpha\delta$ -sites by -1 and -0.3 kcal/mol, respectively ($\Delta G = zF\psi$). The greater stabilization at the $\alpha\gamma$ -site is consistent with the larger number of negative charges in the vicinity of the binding site supplied by the γ -subunit. Examination of the homology structure used in the computations in this article revealed 21 acidic and 16 basic residues within 20 \AA of the NBD-5-AC quaternary ammonium at the $\alpha\gamma$ -binding site, and 17 acidic and 15 basic residues at the $\alpha\delta$ -binding site. Although several charged residues are in loops F, which do not have a structural basis in the AChBP for their conformation, the difference in charge numbers are consistent with the differences in the measured potentials.

Despite the stronger, long-range electrostatic interaction at the $\alpha\gamma$ -site, the desensitized state of the nAChR displays threefold higher affinity at the $\alpha\delta$ -site for ACh and for its fluorescent analog DC6C (8). Differences in agonist affinity between the two sites have been ascribed to γ K34, γ F172, γ E57 and γ C115 for the mouse nAChR (44), but the first two residues appear to primarily affect affinity in the resting state, rather than in the desensitized state, and the second two residues do not involve charge changes. Given the uncertainties in modeling loops F of the binding site structures, we cannot exclude other direct or indirect determinants of affinity differences. Nevertheless, we computed the Poisson-Boltzmann electrostatic potential within the binding pocket at the site of the quaternary ammonium in the absence of ligand, on the homology model at 300 mM ionic strength. This calculation shows a stronger negative potential in the $\alpha\delta$ -site, -87 mV compared with -42 mV in the $\alpha\gamma$ -site (42), that may partly account for the higher affinity of the $\alpha\delta$ -site. When the loop-F charged residues (γ 161–176, δ 164–182) were excluded from the computation, the $\alpha\delta$ -site potential was -84 mV and the $\alpha\gamma$ -site became -33 mV. In this model, the γ F-loop residues had a larger effect on the quaternary ammonium binding site potential, but the influence of loop-F residues was inadequate to explain the difference in potentials at the $\alpha\delta$ - and $\alpha\gamma$ -binding sites. Thus, although $\alpha\gamma$ -site binding has a larger, long-range electrostatic stabilization, $\alpha\delta$ -site binding is preferentially stabilized by shorter-range electrostatic potentials.

Electrostatic effects on nAChR binding kinetics

The fastest component of DC6C binding kinetics reflects diffusion-limited association with the desensitized state of the receptor (7,8,45,46). If long-range electrostatic attraction constitutes a significant mechanism, this rate of binding should be influenced by ionic strength, and the extent to which ionic strength moderates the kinetics should reflect the number and disposition of charged residues (38). The data show a twofold change in the association rate with ionic strength increased up to physiological conditions. This change is reasonably consistent with the observed changes in k_2^+ , relative to k_2^0 , from low to high ionic strength. The kinetic data did not distinguish between the $\alpha\gamma$ - and $\alpha\delta$ -binding sites, but the association rates are similar for the two sites (8) in physiological ionic strength. Nonetheless, it is possible that differences in association rates were missed at low ionic strength conditions and the reported rates reflect an average rate of association.

The change in kinetic rate was analyzed using a Debye-Hückel equation. Increased ionic strength also decreased the potentials measured by DEFET and this change was likewise analyzed by a Debye-Hückel equation. The results of these analyses are compared in Table 4. For NBD-5-AC itself, we obtained a small charge and a radius of 4.4 \AA that likely reflect the distance of the NBD fluorophore from the quaternary ammonium (see Fig. 1). For the nAChR agonist sites, the results differ a good deal, indicating from -0.7 charges to -2.4 . Fitting to the Debye-Hückel formulas may be imprecise because the fitted parameters are correlated, making it difficult to determine either parameter precisely. In addition, most of the dependency that defines the parameters occurs at low ionic strength where experimental error was larger likely because it is more difficult to control pH and ionic conditions.

Comparison of experimental and computed electrostatic potentials

The experimental results on the nAChR agonist sites and on AChE were consistent with the DEFET results calculated on

TABLE 4 Charge distribution at ACh binding sites from ionic strength perturbation

Measurement	Charge (z)	r (\AA)*
NBD-5-AC DEFET	0.13	4.4
nAChR DEFET [†]	-0.7 ± 0.2	3.1 ± 0.7
nAChR, kinetics - Pro [§]	-1.6	7.6
nAChR, kinetics + Pro [§]	-2.4	8.1
AChE [‡]	-9	13

*Mean distance of closest approach of probe to the countercharges.

[†]DEFET experiments with NBD-5-AC bound to nAChR in increasing NaCl (Fig. 4).

[§]Rapid binding of DCC measured with stopped flow (Fig. 5).

[‡]Charge distribution at the AChE active site from Nolte et al. (38) presented for comparison.

the basis of computed Poisson-Boltzmann potentials and numerical integration of DEFET rates, except for the data at the $\alpha\delta$ -site. Observed k_2^x values were higher than calculated k_2^x values in all cases, however, as discussed in Meltzer et al. (14), this was likely because the numerical integration is sensitive to the structure of the complex, to the assigned chelate radius, and to the position of the acceptor dipole. For these calculations, it was assumed that DEFET occurs to the nearest atom of the acceptor fluorophore. It was possible to obtain larger calculated k_2^x values by assigning a smaller chelate radius. A possible source of the discrepancy in raw k_2^x values is other mechanisms of energy transfer, such as charge transfer (17,47) that may have been observed experimentally, but are not Förster energy transfer mechanisms and would not appear in the calculation.

By comparing the voltages on the basis of experimental and computed k_2^x values, we obtain good agreement for free NBD-5AC and for free decidium. This suggests that the algorithm is sound for computing potentials. As discussed (14), most computational and experimental systematic errors will vary similarly for the three k_2^x values (42) and cancel in the voltage calculation. For bound NBD-5AC, the discrepancies observed (Table 2) may arise from the ligand binding models as there is no experimental structure for bound NBD-5AC, although the modeling was apparently unambiguous. In the context of decidium bound to AChE, where the computation was based on a crystal structure, we observed good agreement for all aspects of the measurements.

The electrostatic potential at the AChE active site entrance

The role of the electrostatic potential in attracting ACh to the active site of AChE has been extensively characterized and serves as a benchmark for understanding electrostatic effects on ligand association. The experimental results were consistent with the expected values computed from the k_2^x values, based on the potential computed by continuum Poisson-Boltzmann electrostatics in UHBD. The experimental and computed values agreed to within 30% and this discrepancy was consistent for free decidium, AChE-bound decidium in low ionic strength, and AChE-bound decidium in high ionic strength buffer. The better overall consistency may arise because the crystal structure for bound decidium provides a better basis for the computational estimate than computer-docked ligand-receptor structures. Another possible source of discrepancies between experimental and computational determinations of energy transfer rates and local potentials is an additional mode(s) of Tb^{3+} chelate deexcitation by collisional quenching or electron transfer that is not accounted for in the computational simulations of dipolar energy transfer (47). Nevertheless, the substantial agreement between the experimental and computational results suggests that continuum electrostatic calculations provide a sound basis for determining long-range electrostatic interactions in this instance.

We did not compute the potential in the absence of ligand to gauge the long-term electrostatics, as this has been characterized thoroughly by others (2,4,48). Nonetheless, the fourfold change in k_2^x from neutral to positive, at low ionic strength is similar to the sixfold change seen in rates computed from Brownian dynamics simulations of the association rate of AChE (3) at zero ionic strength. The change in k_2^x values with charge at high ionic strength, about twofold, is also similar to Brownian dynamics simulations and with the observed changes in rates of binding and reaction seen in charge-mutated AChE (4).

CONCLUSIONS

We have determined the contribution of long-range electrostatics to the energy of binding to the nAChR agonist binding sites to be -0.3 and -1 kcal/mol at the $\alpha\delta$ - and $\alpha\gamma$ -sites. We further conclude that the higher desensitized state affinity of agonists to the $\alpha\delta$ -site may be due to short-range electrostatic stabilization at the quaternary ammonium. The experiments on AChE are consistent with previous characterization of the electrostatic properties of this enzyme and its effect on enzymatic activity and the rate of binding.

The overall consistency between the potentials determined from experimental and calculated DEFET rates for AChE and, to a lesser extent, for the nAChR agonist sites, differs from the larger, twofold discrepancies observed for the channel (14). Computation of electrostatics in the confines of a narrow channel where the channel dimensions approach that of the Debye length of the solvent have been argued to overestimate the screening effect of ions (20) because the channel dimensions partly exclude the presence of counterions. However, in that case, it would suggest that computation would underestimate the effective potential and its effect on DEFET, especially at high ionic strength. Instead the computed potentials overestimated the experimentally observed potentials (14), and in both cases, ionic strength had substantial effects on the potential. Lack of screening within the vestibule of the channel does not explain these effects. The source of the discrepancy, therefore, remains to be resolved.

The authors thank Manali Joshi for fruitful scientific discussions regarding the computational work.

This work was supported by U.S. Public Health Service grants RO1-NS 35212 (S.E.P.) and RO1-EY07981 (T.G.W.) and by grants Q-1406 (S.E.P.), E-1497 (J.M.B.), and Q-0035 (T.G.W.) from The Robert A. Welch Foundation and by funding from National Aeronautics Space Administration through the University Research Center at Texas Southern University (J.M.B.). R.H.M. was supported by training grants T32-HL07676 to the Department of Molecular Physiology and Biophysics and T32-GM088280 to the Houston Area Molecular Biophysics Program.

REFERENCES

1. Ripoll, D. R., C. H. Faerman, P. H. Axelsen, I. Silman, and J. L. Sussman. 1993. An electrostatic mechanism for substrate guidance

- down the aromatic gorge of acetylcholinesterase. *Proc. Natl. Acad. Sci. USA.* 90:5128–5132.
2. Tan, R. C., T. N. Truong, J. A. McCammon, and J. L. Sussman. 1993. Acetylcholinesterase: electrostatic steering increases the rate of ligand binding. *Biochemistry.* 32:401–403.
 3. Tara, S., A. H. Elcock, P. D. Kirchhoff, J. M. Briggs, Z. Radic, P. Taylor, and J. A. McCammon. 1998. Rapid binding of a cationic active site inhibitor to wild type and mutant mouse acetylcholinesterase: Brownian dynamics simulation including diffusion in the active site gorge. *Biopolymers.* 46:465–474.
 4. Radic, Z., P. D. Kirchhoff, D. M. Quinn, J. A. McCammon, and P. Taylor. 1997. Electrostatic influence on the kinetics of ligand binding to acetylcholinesterase. Distinctions between active center ligands and fasciculin. *J. Biol. Chem.* 272:23265–23277.
 5. Stauffer, D. A., and A. Karlin. 1994. Electrostatic potential of the acetylcholine binding sites in the nicotinic receptor probed by reactions of binding-site cysteines with charged methanethiosulfonates. *Biochemistry.* 33:6840–6849.
 6. Addona, G. H., S. H. Andrews, and D. S. Cafiso. 1997. Estimating the electrostatic potential at the acetylcholine receptor agonist site using power saturation EPR. *Biochim. Biophys. Acta.* 1329:74–84.
 7. Song, X. Z., and S. E. Pedersen. 2000. Electrostatic interactions regulate desensitization of the nicotinic acetylcholine receptor. *Biophys. J.* 78:1324–1334.
 8. Song, X. Z., I. E. Andreeva, and S. E. Pedersen. 2003. Site-selective agonist binding to the nicotinic acetylcholine receptor from *Torpedo californica*. *Biochemistry.* 42:4197–4207.
 9. Zhong, W., J. P. Gullivan, Y. Zhang, L. Li, H. A. Lester, and D. A. Dougherty. 1998. From ab initio quantum mechanics to molecular neurobiology: a cation- π binding site in the nicotinic receptor. *Proc. Natl. Acad. Sci. USA.* 95:12088–12093.
 10. Brejc, K., W. J. van Dijk, R. V. Klaassen, M. Schuurmans, J. van Der Oost, A. B. Smit, and T. K. Sixma. 2001. Crystal structure of an ACh-binding protein reveals the ligand-binding domain of nicotinic receptors. *Nature.* 411:269–276.
 11. Celie, P. H., S. E. van Rossum-Fikkert, W. J. van Dijk, K. Brejc, A. B. Smit, and T. K. Sixma. 2004. Nicotine and carbamylcholine binding to nicotinic acetylcholine receptors as studied in AChBP crystal structures. *Neuron.* 41:907–914.
 12. Unwin, N. 2005. Refined structure of the nicotinic acetylcholine receptor at 4Å resolution. *J. Mol. Biol.* 346:967–989.
 13. Meltzer, R. H., M. M. Lurtz, T. G. Wensel, and S. E. Pedersen. 2006. Nicotinic acetylcholine receptor channel electrostatics determined by diffusion-enhanced luminescence energy transfer. *Biophys. J.* 91:1315–1324.
 14. Meltzer, R. H., W. Vila-Carriles, J. O. Ebalunode, J. M. Briggs, and S. E. Pedersen. 2006. Computed pore potentials of the nicotinic acetylcholine receptor. *Biophys. J.* 91:1325–1335.
 15. Wensel, T. G., and C. F. Meares. 1983. Electrostatic properties of myoglobin probed by diffusion-enhanced energy transfer. *Biochemistry.* 22:6247–6254.
 16. Wensel, T. G. 1984. Energy transfer studies of proteins and nucleic acids (electrostatics, intercalators, DNA). Dissertation. University of California, Davis, CA.
 17. Wensel, T. G., C. H. Chang, and C. F. Meares. 1985. Diffusion-enhanced lanthanide energy-transfer study of DNA-bound cobalt(III) bleomycins: comparisons of accessibility and electrostatic potential with DNA complexes of ethidium and acridine orange. *Biochemistry.* 24:3060–3069.
 18. Wensel, T. G., C. F. Meares, V. Vlachy, and J. B. Matthew. 1986. Distribution of ions around DNA, probed by energy transfer. *Proc. Natl. Acad. Sci. USA.* 83:3267–3271.
 19. Northrup, S. H., T. G. Wensel, C. F. Meares, J. J. Wendoloski, and J. B. Matthew. 1990. Electrostatic field around cytochrome c: theory and energy transfer experiment. *Proc. Natl. Acad. Sci. USA.* 87:9503–9507.
 20. Moy, G., B. Corry, S. Kuyucak, and S. H. Chung. 2000. Tests of continuum theories as models of ion channels. I. Poisson-Boltzmann theory versus Brownian dynamics. *Biophys. J.* 78:2349–2363.
 21. Waksman, G., M. C. Fournie-Zaluski, and B. Roques. 1976. Synthesis of fluorescent acylcholines with agonistic properties: pharmacological activity on Electrophorus electroplaque and interaction in vitro with Torpedo receptor-rich membrane fragments. *FEBS Lett.* 67:335–342.
 22. Meyers, H. W., R. Jurss, H. R. Brenner, G. Fels, H. Prinz, H. Watzke, and A. Maelicke. 1983. Synthesis and properties of NBD-n-acylcholines, fluorescent analogs of acetylcholine. *Eur. J. Biochem.* 137:399–404.
 23. Jurss, R., H. Prinz, and A. Maelicke. 1979. NBD-5-acetylcholine: fluorescent analog of acetylcholine and agonist at the neuromuscular junction. *Proc. Natl. Acad. Sci. USA.* 76:1064–1068.
 24. Berman, H. A., M. M. Decker, M. W. Nowak, K. J. Leonard, M. McCauley, W. M. Baker, and P. Taylor. 1987. Site selectivity of fluorescent bisquaternary phenanthridinium ligands for acetylcholinesterase. *Mol. Pharmacol.* 31:610–616.
 25. Berman, J. D., and M. Young. 1971. Rapid and complete purification of acetylcholinesterases of electric eel and erythrocyte by affinity chromatography. *Proc. Natl. Acad. Sci. USA.* 68:395–398.
 26. Pedersen, S. E., E. B. Dreyer, and J. B. Cohen. 1986. Location of ligand-binding sites on the nicotinic acetylcholine receptor alpha-subunit. *J. Biol. Chem.* 261:13735–13743.
 27. Sobel, A., M. Weber, and J.-P. Changeux. 1977. Large-scale purification of the acetylcholine-receptor protein in its membrane-bound and detergent extracted forms from *Torpedo marmorata* electric organ. *Eur. J. Biochem.* 80:215–224.
 28. Taylor, P., J. W. Jones, and N. M. Jacobs. 1974. Acetylcholinesterase from *Torpedo*: characterization of an enzyme species isolated by lytic procedures. *Mol. Pharmacol.* 10:78–92.
 29. Laemmli, U. K. 1970. Cleavage of structural proteins during the assembly of the head of bacteriophage T4. *Nature.* 227:680–685.
 30. Ellman, G. L., K. D. Courtney, V. Andres Jr., and R. M. Feather-Stone. 1961. A new and rapid colorimetric determination of acetylcholinesterase activity. *Biochem. Pharmacol.* 7:88–95.
 31. Lamture, J. B., Z. H. Zhou, A. S. Kumar, and T. G. Wensel. 1995. Luminescence properties of terbium(III) complexes with 4-substituted dipicolinic acid analogs. *Inorg. Chem.* 34:864–869.
 32. Bourne, Y., P. Taylor, Z. Radic, and P. Marchot. 2003. Structural insights into ligand interactions at the acetylcholinesterase peripheral anionic site. *EMBO J.* 22:1–12.
 33. Sussman, J. L., M. Harel, F. Frolow, L. Varon, L. Toker, A. H. Futerman, and I. Silman. 1988. Purification and crystallization of a dimeric form of acetylcholinesterase from *Torpedo californica* subsequent to solubilization with phosphatidylinositol-specific phospholipase C. *J. Mol. Biol.* 203:821–823.
 34. Bashford, D., and M. Karplus. 1990. pKa's of ionizable groups in proteins: atomic detail from a continuum electrostatic model. *Biochemistry.* 29:10219–10225.
 35. Madura, J. D., J. M. Briggs, R. C. Wade, M. E. Davis, B. A. Luty, A. Ilin, J. Antosiewicz, M. K. Gilson, B. Bagheri, L. R. Scott, and J. A. McCammon. 1995. Electrostatics and diffusion of molecules in solution - simulations with the University of Houston Brownian dynamics program. *Comput. Phys. Commun.* 91:57–95.
 36. Papineni, R. V., and S. E. Pedersen. 1997. Interaction of d-tubocurarine analogs with the mouse nicotinic acetylcholine receptor. Ligand orientation at the binding site. *J. Biol. Chem.* 272:24891–24898.
 37. Pedersen, S. E., M. M. Lurtz, and R. V. Papineni. 1999. Ligand binding methods for analysis of ion channel structure and function. *Methods Enzymol.* 294:117–135.
 38. Nolte, H. J., T. L. Rosenberry, and E. Neumann. 1980. Effective charge on acetylcholinesterase active sites determined from the ionic strength dependence of association rate constants with cationic ligands. *Biochemistry.* 19:3705–3711.

39. Horrocks, W. D., Jr., and D. R. Sudnick. 1979. Lanthanide ion probes of structure in biology. laser-induced luminescence decay constants provide a direct measure of the number of metal-coordinated water molecules. *J. Am. Chem. Soc.* 101:334–340.
40. Neubig, R. R., and J. B. Cohen. 1979. Equilibrium binding of [3H]tubocurarine and [3H]acetylcholine by Torpedo postsynaptic membranes: stoichiometry and ligand interactions. *Biochemistry*. 18: 5464–5475.
41. Pedersen, S. E., and J. B. Cohen. 1990. d-Tubocurarine binding sites are located at alpha-gamma and alpha-delta subunit interfaces of the nicotinic acetylcholine receptor. *Proc. Natl. Acad. Sci. USA*. 87:2785–2789.
42. Meltzer, R. H. 2004. Protein Electrostatics and the Function of the Nicotinic Acetylcholine Receptor. Baylor College of Medicine, Houston, TX.
43. Zhou, Y., J. H. Morais-Cabral, A. Kaufman, and R. MacKinnon. 2001. Chemistry of ion coordination and hydration revealed by a K⁺ channel-Fab complex at 2.0 Å resolution. *Nature*. 414:43–48.
44. Prince, R. J., and S. M. Sine. 1996. Molecular dissection of subunit interfaces in the acetylcholine receptor. Identification of residues that determine agonist selectivity. *J. Biol. Chem.* 271:25770–25777.
45. Heidmann, T., J. Bernhardt, E. Neumann, and J. P. Changeux. 1983. Rapid kinetics of agonist binding and permeability response analyzed in parallel on acetylcholine receptor rich membranes from Torpedo marmorata. *Biochemistry*. 22:5452–5459.
46. Raines, D. E., and N. S. Krishnan. 1998. Transient low-affinity agonist binding to Torpedo postsynaptic membranes resolved by using sequential mixing stopped-flow fluorescence spectroscopy. *Biochemistry*. 37:956–964.
47. Meares, C. F., S. M. Yeh, and L. Stryer. 1981. Exchange interaction contribution to energy transfer between ions in the rapid-diffusion limit. *J. Am. Chem. Soc.* 103:1607–1609.
48. Antosiewicz, J., S. T. Wlodek, and J. A. McCammon. 1996. Acetylcholinesterase: role of the enzyme's charge distribution in steering charged ligands toward the active site. *Biopolymers*. 39: 85–94.